journal

J. Am. Ceram. Soc., 1–7 (2011)
DOI: 10.1111/j.1551-2916.2011.04999.x

Determination of the Solubility of Tin in Indium Oxide Using *In Situ* and *Ex Situ* X-Ray Diffraction

G. B. González,[‡,†,*] T. O. Mason,[§,*] J. S. Okasinski,[¶] T. Buslaps,[‖] and V. Honkimäki[‖]

[‡]Department of Physics, DePaul University, Chicago, Illinois 60614

[§]Department of Materials Science and Engineering, Northwestern University, Evanston, Illinois 60208

[¶]Advanced Photon Source, Argonne National Laboratory, Argonne, Illinois 60439

[‖]Experiments Division, European Synchrotron Radiation Facility, F- 38043 Grenoble, France

A novel approach to determine the thermodynamic solubility of tin in indium oxide via the exsolution from tin overdoped nano-ITO powders is presented. High-energy, *in situ* and *ex situ* synchrotron X-ray diffraction was utilized to study the solubility limit at temperatures ranging from 900°C to 1375°C. The tin exsolution from overdoped nanopowders and the formation of $In_4Sn_3O_{12}$ were observed *in situ* during the first 4–48 h of high-temperature treatment. Samples annealed between 900°C and 1175°C were also studied *ex situ* with heat treatments for up to 2060 h. Structural results obtained from Rietveld analysis include compositional phase analysis, atomic positions, and lattice parameters. The tin solubility in In_2O_3 was determined using the phase analysis compositions from X-ray diffraction and the elemental compositions obtained from X-ray fluorescence. Experimental complications that can lead to incorrect tin solubility values in the literature are discussed.

I. Introduction

Sn-doped indium oxide materials are widely used in commercial applications due to their superior optical and electrical properties. Indium-tin oxide (ITO) materials can be prepared as thin films, powders, and single crystals. Thin films, supersaturated coprecipitates, and nanomaterials can be synthesized with substantial amounts of tin in solution (up to 40 at.% Sn) while remaining phase-pure bixbyite.[1,2] On the other hand, as the present work shows, bulk powder samples, which are materials in thermodynamic equilibrium, exhibit much smaller solid solubilities. For powders, the incorporation of Sn into the indium oxide lattice requires either high-temperature sintering or other processes, which may result in supersaturated materials that can then be brought into equilibrium by high-temperature annealing. Coprecipitation and physical vapor synthesis are two of the processes that can synthesize phase-pure supersaturated powders.

Several authors have reported the solubility of tin in indium oxide at different temperatures on quenched specimens prepared *ex situ*.[3–11] The reported temperatures range from 600°C[4] upto 1650°C.[9] The solubility limits and phase boundaries disagree dramatically among these reports. Another discrepancy exists on the reported structure, stoichiometry and temperature at which a fluorite-derived, intermediate phase forms. This phase has been reported as pyrochlore $In_2Sn_2O_{7-x}$ with a lattice parameter of 10.226 Å[5] at temperatures higher than 1200°C; cubic with a lattice parameter of 10.21 Å[6,7] at temperatures higher than 1250°C; hexagonal with lattice parameters a = 9.5 Å and c = 17.5 Å at 1552°C[8]; and rhombohedral $In_4Sn_3O_{12}$ at 1325°C,[9] 1370°C, [10] 1400°C,[11] and 1552°C.[8]

Two recent articles reported on solid solubilities of tin in indium oxide powder samples.[9,10] Ohya *et al.*[10] studied the solid solubility between 1000°C and 1500°C using powders prepared with either tin alkoxide solutions and In_2O_3 powder or mixed indium and tin alkoxides. The solubility limits determined from X-ray diffraction were 0.5, 2.0, 3.5, and 5.0 at.% at 1000°C, 1300°C, 1400°C, and 1500°C, respectively. The samples were annealed for 1200 h at 1000°C, 30 h at 1300°C, and 15 h at both 1400°C and 1500°C. The presence of the $In_4Sn_3O_{12}$ phase was observed at 1380°C, but not at 1360°C.

Heward and Swenson[9] studied the phase diagram in 800°C–1650°C temperature range using powder samples prepared from bulk In_2O_3 and SnO_2 materials. The materials were annealed in air for 10 h or more, depending on the temperature. At high temperatures, the samples were buried inside loose powder of the same composition to slow down volatilization. X-ray diffraction was used to identify the phases, and the indium and tin concentrations were determined using wavelength-dispersive spectroscopy and electron probe micronalaysis. At 800°C, the authors could not detect any solubility within experimental accuracy of the EPMA (~0.5 mol%). For temperatures lower than 1325°C, only ITO and SnO_2 phases were observed. For temperatures between 1350°C and 1650°C, ITO, SnO_2, and an intermediate phase indexed as $In_4Sn_3O_{12}$ were observed. At 1650°C, an orthorhombic In_2SnO_5 phase was observed.

As the strongest peaks of fluorite-derived phases have similar d-spacings to those of the bixbyite structure, it can be difficult to accurately index these phases and sometimes even to detect them in small concentrations. Using high-energy X-ray diffraction, we have carefully characterized the stoichiometry, kinetics, and transformation temperature of the $In_4Sn_3O_{12}$ phase.[12] This phase formed at 1345°C, and using X-ray diffraction and X-ray fluorescence, we confirmed its stoichiometry and studied the behavior of the lattice parameters as a function of temperature.

The present study reports solubility limit results in the 900°C–1375°C temperature range, obtained from high-energy X-ray diffraction data. Two different nanopowder ITO batches with a concentration near 9 cation% Sn were used as starting materials and isothermally annealed at temperatures

P. Gouma—contributing editor

Manuscript No. 30225. Received August 23, 2011; approved November 07, 2011.
TOM and GBG acknowledge support from the NSF MRSEC program at Northwestern University under grant no. DMR-0520513.
*Member, The American Ceramic Society.
[†]Author to whom correspondence should be addressed. e-mail: ggonza18@depaul.edu.

Table I. *In Situ* Samples

Sample	Batch	Temperature (°C)	Time (h)	Postanneal†		Sn in ITO‡ cation%	Final XRF		Sn in ITO§ cation%
				SnO_2	$In_4Sn_3O_{12}$		In	Sn	
1	NT	1000	48	6.8	0	3.0 (2)	Not measured		
2	AC	1000	43	6.2	0	3.0 (2)	91.2	8.8	2.7 (2)
3	NT	1100	36	8.2	0	1.7 (1)	90.6	9.4	2.0 (2)
4	AC	1100	36	7.4	0	1.8 (1)	91.2	8.8	2.0 (2)
5	NT	1200	40	7.7	0	2.1 (1)	90.8	9.2	2.1 (2)
6	AC	1200	42	7.4	0	1.9 (1)	91.4	8.6	2.0 (2)
7	NT	1250	15	7.5	0	2.3 (2)	90.6	9.4	2.6 (2)
8	AC	1250	15	7.0	0	2.3 (2)	91.4	8.6	2.3 (2)
9		1335	45	43.6	0	2.50 (4)	57.0	43.0	
10	AC	1365	14	0.1	7.0	2.9 (1)*	94.2	5.8	2.8 (2)
11	NT	1365	10	0.1	9.1	3.1 (1)*	93.9	6.1	3.3 (2)
12	NT	1375	4	0.1	11.4	2.9 (1)*	92.5	7.5	3.0 (2)
13	NT	1375	13	0.01	2.4	3.4 (1)*	96.5	3.5	3.4 (2)

†SnO_2 and $In_4Sn_3O_{12}$ are expressed as weight percentages. The ITO phase constitutes the remaining weight percent for each sample.
‡Obtained from XRD results, assuming negligible solubility of In in SnO_2 and no evaporation, except for samples 10–13 where Sn preferentially evaporated.
§Calculated from XRF and XRD results.

between 900°C and 1375°C. The crystal structure and phase fractions of all phases present were determined using Rietveld analysis. In addition, the indium and tin compositions of the samples were independently measured with X-ray fluorescence analysis to corroborate the cation stoichiometry of the phases in the postannealed samples.

II. Experiment

(1) Sample Preparation

Two commercially produced nanocrystalline ITO powder batches were obtained for these experiments. The powder labeled NT (Nanophase Technologies, Romeoville, IL) had a tin concentration of 9.2(2) cation% and an average particle size of 18 nm. The powder AC (Aldrich Chemical Co., Milwaukee, WI) had a tin concentration of 8.6(2) cation% and an average grain size of 45 nm. To study the solubility limit at 1335°C, nano-In_2O_3 99.999% and nano-SnO_2 99.995+% powders (Aldrich Chemical Co.) were combined to obtain a homogenous mixture of 54.47 wt% In_2O_3 and 45.53 wt% SnO_2. The grain size of the starting materials for this sample was ~20 nm for tin oxide and 40 nm for indium oxide. The chemical compositions of the powders were determined from X-ray fluorescence (XRF) measurements. The particle sizes were obtained from SEM and X-ray diffraction.

The powders for *in situ* measurements were homogenized with acetone in a mortar and pestle and pressed into pellets 5 mm in diameter and 1 mm thick using a hydraulic press and a pressure of 150 MPa. The samples for *ex situ* measurements were pressed at 150 MPa and then isostatically pressed at 280 MPa. The dimensions of these pellets were 6.35 mm (0.25 in.) in diameter and ~2 mm in thickness. The samples were buried in sacrificial powder and sintered in alumina crucibles for various times, depending on the temperature, and quenched to room temperature. The density of the pellets was ~50% of the theoretical value. Samples descriptions are listed in Tables I–V.

(2) X-Ray Powder Diffraction Experiments

High-energy X-ray experiments were conducted at the ID15-B beamline of the European Synchrotron Radiation Facility (ESRF). As high-energy radiation can penetrate deep into materials, the diffraction data collected in transmission mode are representative of the bulk sample.

A Si 511 cylindrically bent Laue crystal monochromatized the X-ray radiation to an energy of ~90 keV. The exact X-ray energy and instrumental resolution were calibrated during each experiment with the LaB_6 NIST standard reference material 660a. The incident beam was 200 μm × 200 μm. Entire Debye rings were collected in the forward direction using a two-dimensional MAR345 image plate with a diameter of 345 mm and a 2300 × 2300 pixel array. The sample-to-detector distance was determined for each sample independently and was ~1300 mm to obtain well-resolved peaks.

Diffraction data for the first 4–48 h of sample annealing above 1000°C were collected *in situ* using a furnace constructed from an inner alumina cylinder wrapped with a Pt/Rh heating element and surrounded by a water-cooled

Table II. *Ex Situ* NT Samples Annealed at 900°C

Sample	Time (h)	Postanneal XRF	
		In	Sn
14	0	90.59	9.41
15	1	Not measured	
16	4.1	90.61	9.39
17	12.0	90.64	9.36
18	24.0	90.59	9.41
19	164.2	90.59	9.41
19	419.3	Not measured	
20	580.0	Not measured	
20	911.8	Not measured	
20	2061.0	90.56	9.44

Table III. *Ex Situ* NT Samples Annealed at 1000°C

Sample	Time (h)	Postanneal XRF	
		In	Sn
21	0	90.59	9.41
22	0.3	90.65	9.35
23	4.8	90.61	9.39
24	7.0	90.60	9.40
25	18.7	90.64	9.36
26	26.5	90.61	9.39
27	58.8	90.60	9.40
28	147.3	Not measured	
29	375.2	90.60	9.40
28	447.7	Not measured	
28	1163	90.60	9.40

Table IV. *Ex Situ* NT Samples Annealed at 1100°C and 1175°C

			Postanneal XRF	
Sample	Temperature (°C)	Time (h)	In	Sn
30	1100	0	90.63	9.37
31	1100	0.2	90.64	9.36
32	1100	0.7	90.65	9.35
33	1100	4.7	Not measured	
34	1100	120.6	90.59	9.41
35	1100	423.0	90.63	9.37
36	1175	0.1	90.58	9.42
37	1175	9.3	90.58	9.42
38	1175	125.4	90.57	9.43
39	1175	301.1	90.57	9.43

stainless steel jacket. The temperature was controlled by regulating a DC power supply to the Pt/Rh wire with feedback from a thermocouple inside the furnace. A type S thermocouple was mounted in contact with the edge of the sample. The thermocouple readings were measured with a temperature controller (Eurotherm 2408i) and recorded at the same time the diffraction data were being collected. The heating and cooling rates of the furnace were 5°C/min. Diffraction images were taken while the pellet was translating over a 0.4-mm range. The purpose of translating the pellet was to increase the number of grains sampled to obtain a better representation of the sample. The translation of the pellet resulted in a temperature change of less than one degree. Two windows with 1.3 mm and 13 mm in diameters let the incident and diffracted beams, respectively, pass through the furnace while minimizing thermal gradients. Reflections up to *d*-spacings of ~1 Å were collected. The two-dimensional images were integrated and geometrical corrections were applied using programs written in the software MATLAB (The MathWorks, Inc., Natick, MA).

Laboratory X-ray diffraction patterns were also collected using a Scintag diffractometer equipped with a solid-state detector setup to only measure diffraction from the Cu$K\alpha_I$ and $K\alpha_{II}$ lines. The synchrotron and laboratory diffraction patterns were simultaneously analyzed using the Rietveld method[13] with the program FullProf.[14]

The indium and tin concentrations for the pellets were determined with XRF before and after the thermal annealing. A Ge solid-state detector collected all the fluorescence lines from the sample using an incident X-ray energy of ~90 keV. The program X-FLU[15] was used to fit both the primary and secondary fluorescence lines to determine the indium and tin compositions.

III. Results and Discussion

When pellets of tin-oversaturated ITO nanopowder material were sintered at temperatures higher than 500°C, the grains started to grow. The growth rate depended on the temperature, but as a consequence of the growth, secondary SnO_2 phase precipitated, indicating that a bixbyite-pure material having such a high tin concentration was not stable at those high temperatures. This observation was used to study the solubility limits for temperatures 900°C–1375°C. At these and higher temperatures, these nanopowders are overdoped materials, but by growing the particles, the tin content moves toward the equilibrium concentration.

Table I summarizes the temperatures and isothermal annealing times of the samples that were studied *in situ*. The postanneal phase composition of the samples is also shown. Only the tetrahedral tin oxide and bixbyite ITO phases were present for temperatures $\leq$1335°C. At 1365°C and 1375°C, the $In_4Sn_3O_{12}$ phase was also present. These latter samples suffered from evaporation, and the final tin concentration in the samples decreased with annealing time. For example, sample 12 lost ~20% of its initial Sn content after 4 h of annealing at 1375°C, whereas sample 13 suffered the most severe evaporation losing 63% of its initial Sn content after 13 h at this same temperature. The *ex situ* samples, which were annealed up to 1175°C for longer times, did not exhibit any evaporation as seen in Tables II–IV. A summary of the annealing conditions, grain size, phase, and elemental compositions of the samples with the longest annealing treatments is presented in Table V.

The deep penetration of 90 keV X-rays allowed the collection of diffraction patterns from a large volume of grains through the entire thickness of the samples. Uniform radial intensities around the Debye rings indicate random orientation of the grains during growth. The two-dimensional data were radially integrated and fitted. A typical Rietveld refinement is shown in Fig. 1. Table VI contains the refined atomic positions and Rietveld reliability parameters for the samples with the longest annealing times. The Debye–Waller factors and occupational fractions for ITO were fixed to those obtained from a combined synchrotron and neutron diffraction study.[16] The atomic positions in the ITO phase did not change significantly with heat treatment. The Rietveld

Table V. Samples with the Longest Isothermal Annealing Times

			Postanneal[†]			XRF			
Sample	Temperature (°C)	Time (h)	SnO_2	$In_4Sn_3O_{12}$	Sn in ITO[‡] cation%	In	Sn	Sn in ITO[§] cation%	Apparent size (nm)
20	900	2061	7.3 (4)	0	2.6 (1)	90.6	9.4	2.8 (2)	109
28	1000	1163	8.2 (5)	0	1.6 (1)	90.6	9.4	1.9 (2)	208
35	1100	423	8.1 (5)	0	1.8 (1)	90.6	9.4	2.0 (2)	302
39	1175	301	8.0 (3)	0	1.8 (1)	90.6	9.4	2.1 (2)	355
5	1200	40	7.7	0	2.1 (1)	90.8	9.2	2.1 (2)	571
6	1200	42	7.4	0	1.9 (1)	91.4	8.6	2.0 (2)	624
7	1250	15	7.5	0	2.3 (2)	90.6	9.4	2.6 (2)	925
8	1250	15	7.0	0	2.3 (2)	91.4	8.6	2.3 (2)	951
9	1335	45	43.6	0	2.50 (4)	57.0	43.0		RL[¶]
10	1365	14	0.1	7.0	2.9 (1)	94.2	5.8	2.8 (2)	RL[¶]
11	1365	10	0.1	9.1	3.1 (1)	93.9	6.1	3.3 (2)	RL[¶]
12	1375	4	0.1	11.4	2.9 (1)	92.5	7.5	3.0 (2)	RL[¶]
13	1375	13	0.01	2.4	3.4 (1)	96.5	3.5	3.4 (2)	RL[¶]

[†]SnO_2 and $In_4Sn_3O_{12}$ are expressed as weight percentages. The ITO phase constitutes the remaining weight percent for each sample.
[‡]Obtained from XRD results, assuming negligible solubility of In in SnO_2 and no evaporation, except for samples 10–13 where Sn preferentially evaporated.
[§]Calculated from XRF and XRD results.
[¶]RL means resolution limited.

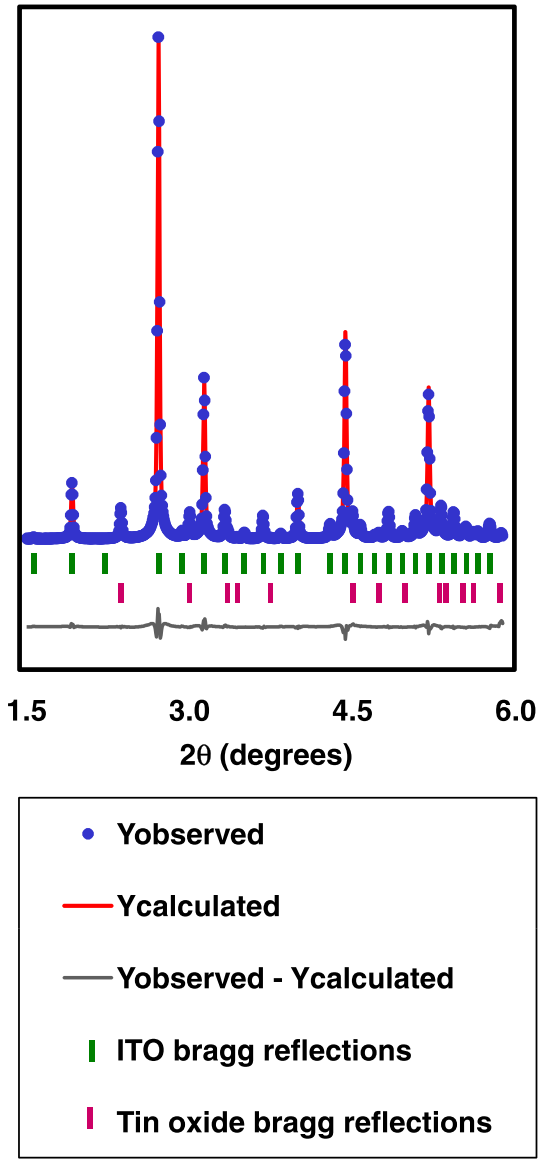

Fig. 1. Rietveld refinement of X-ray synchrotron diffraction data on sample 28 after heating to 1000°C for 1163 h.

agreement factors validate the reliability of the structural results.

The weight fractions of the bixbyite, tetragonal, and rhombohedral phases were also determined from the Rietveld analysis. Figure 2 shows the weight percent of SnO_2 that precipitated from the bixbyite phase from NT *ex situ* samples. The initial concentrations of the Sn-doped indium oxide nanopowders were 9.2(2) cation at.% for NT and 8.6(2) cation at.% for AC samples. From the initial Sn content and the weight fraction of precipitated SnO_2, the concentration of tin remaining in solution in the In_2O_3 lattice can be calculated. For example, for the AC powders, the reaction is as follows:

$$A\left(In_{2-0.172}Sn_{0.172}O_{3+\frac{0.172}{2}}\right) \rightarrow B(SnO_2) + C\left(In_{2-x}Sn_xO_{3+\frac{x}{2}}\right) \quad (1)$$

The resulting tin concentration in the ITO phase for the samples can then be calculated assuming that there is no preferential evaporation of tin or indium and that the tin oxide phase has negligible indium solubility. In Tables I and V, the tin solubility is calculated using this method, except for samples 10–13 where tin evaporation is evident. For these samples, the tin content used was corrected using the XRF measurements. Another method to calculate the tin solubility uses the weight fractions from XRD and the XRF data to match the total tin and indium contents and is presented in the last column of Tables I and V. These two calculation methods were consistent with each other, as shown in the tables. The Sn content in ITO is shown in Fig. 3 for the *ex situ* samples and in Fig. 4 for the *in situ* samples. For the *in situ* samples, it can be seen that even when the initial tin concentrations of the NT and AC samples were different, at later times both curves meet and follow similar patterns. This indicates that regardless of initial tin content, the thermodynamic solubility was reached after long annealing times, as expected.

The lattice parameter of the ITO phase for the *ex situ* samples is plotted in Fig. 5. For sample 9, undoped indium oxide with a grain size of 40 nm, a = 10.1171(2) Å. The unit cell shrinks with decreasing tin in solution. Various authors have reported increases in the lattice parameter of bixbyite phase with increasing tin solid solution.[1,2,5,7,8,10,11] This behavior is at first not apparent, as the cation size of In^{3+} (0.81 Å) is larger than that of Sn^{4+} (0.71 Å). Based on cation size, the lattice parameter is expected to decrease with tin doping. Such a decrease is actually observed for very small concentrations of tin (<1%). Frank and Köstlin[1] proposed that with increasing tin, there is an increased probability of finding Sn species closer to each other, and their effective charges cause repulsion, resulting in lattice parameter expansion.

The refined volume of the tin oxide phase is plotted as a function of precipitated SnO_2 in Fig. 6. For samples with <4 wt% SnO_2, the lattice parameters of this phase were fixed to 71.39 Å,[3] which corresponds to the average of the values refined in this experiment. Figure 6 indicates that within experimental error, the volume of the tin oxide unit cell does not differ significantly from that of undoped SnO_2, regardless of the processing temperature or the amount of tin exsolution. Before annealing sample 9, the lattice parameters of undoped tin oxide with a grain size of 20 nm were a = 4.7378(1) Å and c = 3.1864(1) Å. These parameters correspond to a volume of 71.519(3) Å,[3] which is ~0.18% larger than the average refined volume listed above. Based on cation size, the lattice parameter is expected to increase with indium doping, which is not observed. In addition, several authors have reported negligible solubility of indium in tin oxide.[4,9] Therefore, this study presumes no indium solubility in SnO_2. The Sn-solubility in the ITO phase results would be higher if this assumption is incorrect. For example, assuming that the solubility of indium in tin oxide is 1 cation% at 1000°C, the tin solubility in indium oxide would be 1.7(1) instead of 1.6(1). This small change falls within the uncertainty of the reported results.

The solubility limits of tin in indium oxide for the samples in Table V are inserted in the phase diagram shown in Fig. 7. The data from Ohya *et al.*[10] and Heward and Swenson[9] are also shown for comparison purposes. For temperatures higher than 1350°C, the data agree with the phase boundary of Ohya *et al.*[10] In the 1000°C–1300°C range, the tin solubility limits are higher than those reported by Ohya *et al.*[10] and Heward and Swenson.[9] For the present study, below 1300°C, the tin solubility limit was investigated at 900°C (metastable), 1000°C, 1100°C, 1175°C, 1200°C, and 1250°C, and the phase boundary shows a consistent increasing trend in the tin amount as a function of temperature. Ohya *et al.*[10] only measured tin solubilities at 1000°C and 1300°C, while Heward and Swenson reported results at 800°C, 1000°C, 1200°C, and 1300°C. At 1000°C, similar annealing times were investigated: 1163 h for the present study, 1200 h for Ohya *et al.*,[10] and 840 h for Heward and Swenson.[9] Figures 2, 3, and 5 suggest that the present exsolution at 1000°C reached thermodynamic equilibrium after 375 h. It is possible that

Table VI. Atomic Positions[†] and Rietveld Agreement Factors for Samples Presented in Table V

	Refined atomic positions for bixbyite[‡]				Rietveld indices(%) [§]		
	Cation *d*	Oxygen					
Sample	*x*	*x*	*y*	*z*	R_p	R_{wp}	R_{exp}
20	0.4675 (1)	0.3902 (9)	0.1528 (8)	0.382 (1)	4.32	5.43	3.93
28	0.4669 (1)	0.3904 (9)	0.1532 (9)	0.382 (1)	4.38	5.75	3.98
35	0.4666 (2)	0.3907 (9)	0.1540 (9)	0.382 (1)	4.49	5.92	4.00
39	0.4668 (2)	0.3901 (9)	0.1542 (9)	0.382 (1)	4.56	5.95	5.82
5	0.46791 (7)	0.03918 (6)	0.1532 (5)	0.3844 (7)	1.54	2.20	1.58
6	0.4669 (6)	0.3901 (5)	0.1541 (5)	0.3830 (6)	1.93	2.78	1.28
7	0.46751 (7)	0.3916 (6)	0.1553 (5)	0.3837 (7)	2.69	3.53	2.09
8	0.4669 (7)	0.3910 (5)	0.1547 (5)	0.3842 (6)	2.89	3.84	2.15
9	0.4685 (2)	0.395 (1)	0.155 (1)	0.384 (2)	2.92	4.06	3.59
10	0.4674 (1)	0.3931 (9)	0.1571 (8)	0.3826 (9)	4.42	5.69	1.71
11	0.4674 (1)	0.3928 (9)	0.1558 (8)	0.3840 (9)	4.50	5.74	1.75
12	0.4685 (2)	0.395 (1)	0.156 (1)	0.384 (1)	3.95	5.46	2.11
13	0.4673 (1)	0.3925 (9)	0.1578 (8)	0.381 (1)	4.40	5.68	1.73

[†]Atomic positions for SnO_2 are fixed to $x = y = z = 0$ for tin and $x = y = 0.3014$, $z = 0$ for oxygen.

[‡]Atomic positions for cation *b* are $x = y = z = 0.25$; for cation *d*, the positions are *x*, $y = 0$, $z = 0.25$. The Debye–Waller factors and occupational fractions are fixed to those in Ref. [16].

[§]Rietveld refinement indices for the synchrotron data.

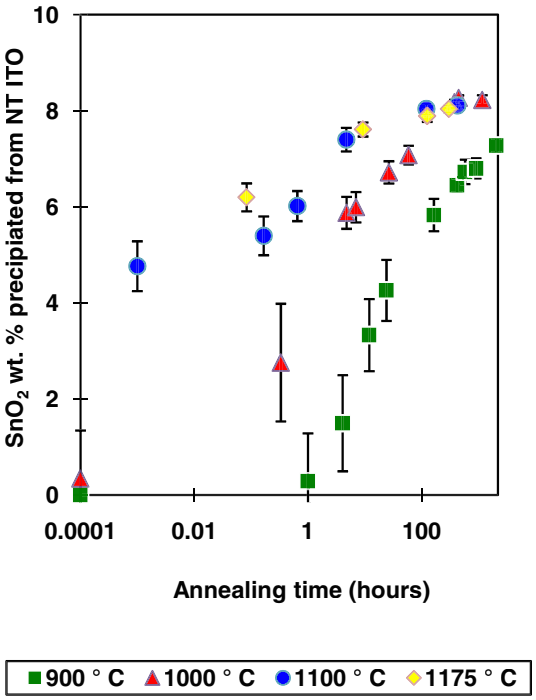

Fig. 2. Tin oxide precipitated from NT *ex situ* samples.

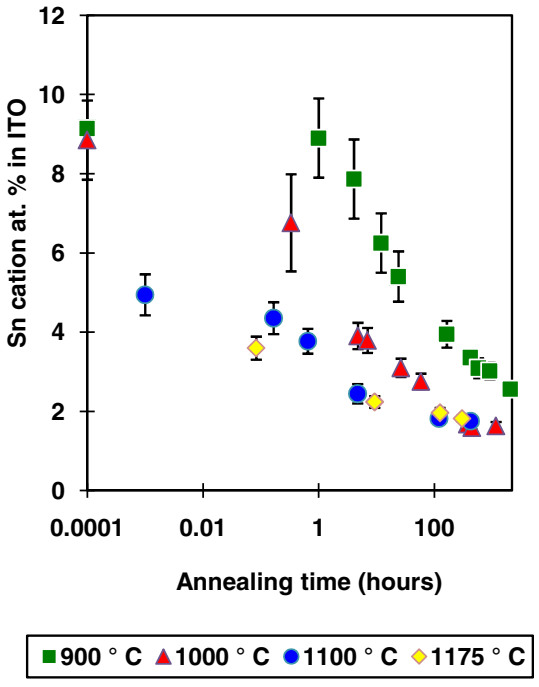

Fig. 3. Tin content in ITO for *ex situ* samples.

thermodynamic equilibrium is reached faster during the exsolution from overdoped nano-ITO powders than in conventional high-temperature solid-state reaction of materials with much larger grain sizes, as followed in Refs. [9,10] where tin dissolves into the In_2O_3 lattice. When the starting materials are of nanosize dimensions, the diffusion may be faster and equilibrium is reached after long annealing times. The present study confirms that stability is reached at all the reported temperatures (except for 900°C) as the tin content reaches a clear plateau. The behavior of the grain size follows a similar trend. Equilibrium was reached after ~120 h for 1100°C and 1175°C; 10 h for 1200°C and 1250°C; and just a few hours for 1335°C, 1365°C, and 1375°C. Further evidence on the accuracy of the present solubilities is supported by the overlap of the tin content for both NT and AC batches at late stages, even when the starting compositions differed by 0.8%. As mentioned before, it is expected that the thermodynamic solubility limit is the same regardless of the initial tin concentrations of the samples.

The data at 900°C do not seem to be in the final stages of the reaction yet. Tin oxide precipitation and grain growth exhibit similar trends: a rapid growth rate region is followed by a regime of much slower rate. The apparent sizes of the crystallites obtained from XRD for the longest annealed samples are found in Table V. The synchrotron experimental setup allowed the size determination of crystallites smaller than 1 μm. Above 1 μm, the size determination using the X-ray peak broadening was not possible due to the instrumental resolution. SEM images were collected for all samples after the heat treatment, and grain sizes were consistent with the XRD results. The SEM images confirm that the particle size of the high-temperature samples was in the micrometer range. For the samples annealed at 900°C, the kinetics

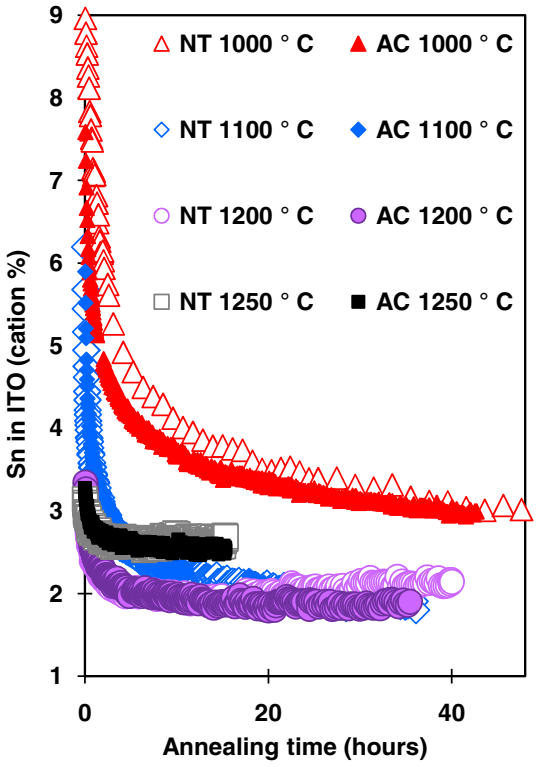

Fig. 4. Tin content in ITO for *in situ* samples 1 through 8.

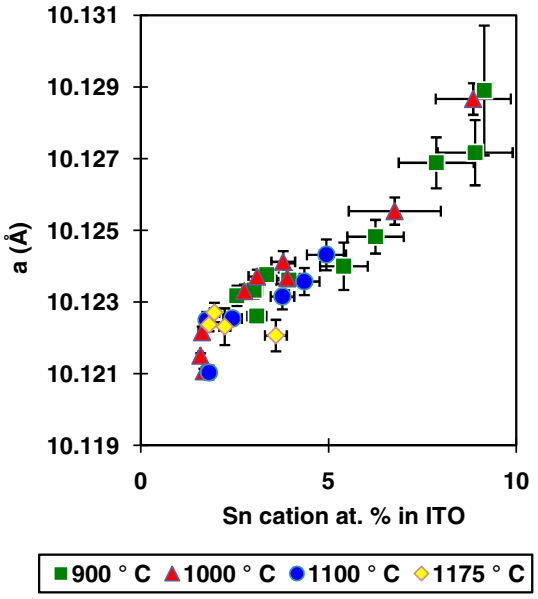

Fig. 5. Lattice parameter of ITO as a function of Sn in solution for samples 14–39.

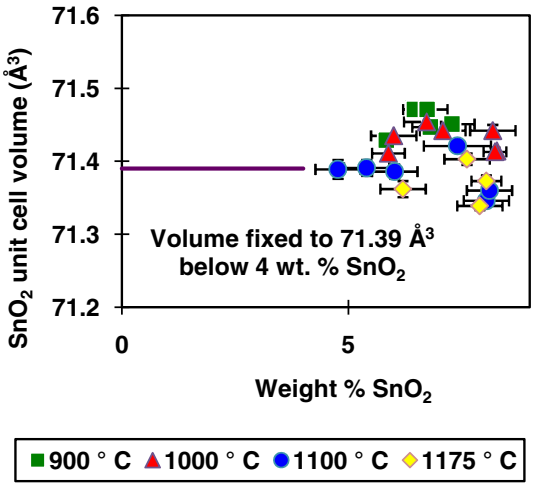

Fig. 6. Volume of the SnO_2 unit cell as a function of tin oxide precipitated from NT *ex situ* samples.

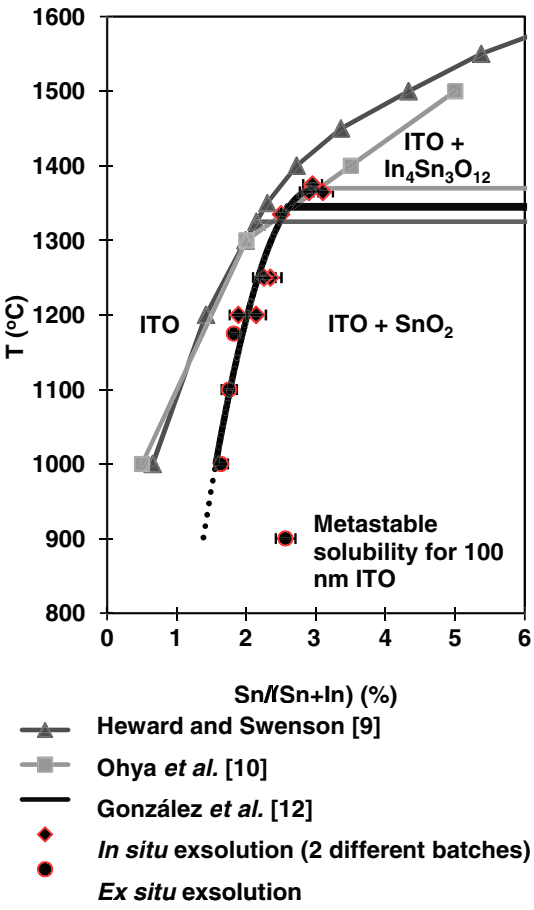

Fig. 7. Thermodynamic solubility of Sn in ITO as a function of temperature, according to Refs. [9,10,12] and this study.

are quite slow, and even after annealing for 2060 h, the particles are ~100 nm and continue growing while more tin oxide precipitates very slowly. For higher temperatures, the ITO grain sizes have attained sizes over 0.2 μm and the tin content has stabilized. It seems reasonable to think that given enough annealing time at 900°C (much more than the 3 months of annealing done in this study), the particle size would grow, and the tin concentration in solution would further decrease to <2 cation% (as shown in the extrapolated boundary).

The formation temperature of $In_4Sn_3O_{12}$ occurs between 1335°C and 1345°C.[12] Only tetragonal and bixbyite phases were present in the sample heated at 1335°C, even after annealing for 45 h. The hexagonal phase formed at 1345°C, after 4.3 h. As mentioned before, the evaporation of tin became significant at higher temperatures and extended annealing times. For the samples heated at 1365°C and 1375°C, the fraction of $In_4Sn_3O_{12}$ phase decreased, whereas the fraction of ITO started to increase at later times. These observations indicate that tin evaporation is occurring because the SnO_2 phase does not reappear once it has been exhausted. As $In_4Sn_3O_{12}$ has higher tin concentration than ITO, the evaporation of tin causes the decrease of $In_4Sn_3O_{12}$,

and the remaining indium and oxygen recombine to form more of the bixbyite phase. The evaporation of tin in specimens annealed at high temperatures and long times was confirmed by X-ray fluorescence measurements collected before and after the annealing processes. Preferential evaporation of tin at high temperatures may result in the inference of incorrect solid solubilities in the absence of chemical composition analysis.

IV. Conclusions

High-energy *in situ* and *ex situ* X-ray diffraction was used to study the solid solubility of SnO_2 in In_2O_3 under isothermal annealing conditions of overdoped nanopowders at temperatures ranging from 900°C to 1375°C. Phase fractions and elemental compositions from X-ray diffraction and X-ray fluorescence results were used to study the exsolution of tin oxide from supersaturated nanopowders during grain growth and equilibration. For samples annealed below 1335°C, the $In_4Sn_3O_{12}$ phase was absent. The results also indicate that in the temperature range studied, the indium solubility in SnO_2 remains the same, and appears to be negligible, as suggested by previous studies.[4,9]

The experiments performed during the present study suggest that the solubility limits of tin in indium oxide are about 2 cation% when the temperature is below 1200°C. The tin solubility increases with temperature and reaches 3 cation% at 1375°C. These values are smaller than what several references[3–8,11] report. For temperatures higher than 1350°C, the present data agree with the phase boundary of Ohya *et al.*[10] In the 1000°C –1300°C range, the tin solubility limits are higher than those reported by Ohya *et al.*[10] and Heward and Swenson.[9]

One reason for disagreement between the various literature reports is the presence of metastable tin concentrations. It is possible to tin-dope indium oxide using various techniques, which may not always result in stable materials. Materials would then need to be equilibrated at the desired temperature, and reaching equilibrium at lower temperatures is not always achieved, as observed in the present study at 900°C. Sluggish kinetics can require extensive annealing times to reach equilibrium. On the other hand, evaporation of Sn at high temperatures could result in the overestimation of the tin solubility limits. Moreover, accurate structural determination of X-ray patterns having similar phases represents a problem resulting in incorrect tin solubility limits, as discussed in our previous study.[12] Intermediate, high-temperature phases that are fluorite-derived have X-ray diffraction patterns that are very similar to bixbyite ITO. Their strongest peaks have almost identical *d*-spacings and complicate phase determination. Thus, if a sample contains bixbyite solid solution plus only a small amount of these phases, peak overlap may result in the incorrect phase composition of the sample, and erroneous lattice parameters as well. In the worst-case scenario, these secondary phases are not detected at all, and the sample is assumed to be phase-pure ITO bixbyite with all the tin in solution. Finally, the incorrect composition determination in ITO materials could also result in incorrect tin solubility limits. The present study has carefully monitored the tin exsolution from supersaturated ITO samples and has accounted for all these experimental complications. Due to the precision and penetration depth of the high-energy X-ray diffraction technique and the measurement of the indium and tin contents via X-ray fluorescence, the authors believe their phase boundary to be the true equilibrium phase boundary for Sn-doped In_2O_3.

Acknowledgments

This work was performed at ID15-B, the High-Energy Beamline of the European Synchrotron Radiation Facility (ESRF) and at the J B Cohen X-ray Laboratory at Northwestern University. The authors acknowledge Dr. Irina Snireva for her help with SEM images.

References

[1]G. Frank and H. Köstlin, "Electrical Properties and Defect Model of Tin-Doped Indium Oxide Layers," *Appl. Phys. A*, **27**, 197–206 (1982).
[2]Ph. Parent, H. Dexpert, G. Tourillon, and J.-M. Grimal, "Structural Study of Tin-Doped Indium Oxide Thin Films Using X-Ray Absorption Spectroscopy and X-Ray Diffraction I. Description of the Indium Site," *J. Electrochem. Soc.*, **139**, 276–81 (1992).
[3]G. Frank, H. Köstlin, and A. Rabenau, "X-Ray and Optical Measurements in the In_2O_3-SnO_2 System," *Phys. Stat. Sol. A*, **52**, 231–8 (1979).
[4]G. Frank, L. Brock, and H. D. Bausen, "The Solubilities of Sn in In_2O_3 and of In in SnO_2 Crystals Grown from Sn-In Melts," *J. Cryst. Growth*, **36**, 179–80 (1976).
[5]A. E. Solov'eva and V. A. Zhdanov, "Features of the Interaction of Indium Oxide with SnO_2," *Inorg. Mater.*, **21**, 828–31 (1985).
[6]H. Enoki, J. Echigoya, and H. Suto, "The Intermediate Compound in the In_2O_3-SnO_2 System," *J. Mater. Sci.*, **26**, 4110–5 (1991).
[7]H. Enoki and J. Echigoya, "Electron Microscopy Study of the $3SnO_2$. $2In_2O_3$ Intermediate Compound," *Phys. Stat. Sol. A*, **132**, K1–5 (1992).
[8]J. L. Bates, C. W. Griffin, D. D. Marchant, and J. E. Garnier, "Electrical Conductivity, Seebeck Coefficient, and Structure of In_2O_3-SnO_2," *Am. Ceram. Soc. Bull.*, **65**, 673–8 (1986).
[9]W. J. Heward and D. J. Swenson, "Phase Equilibria in the Pseudo-Binary In_2O_3-SnO_2 System," *J. Mater. Sci.*, **42**, 7135–40 (2007).
[10]Y. Ohya, T. ITO, M. Kaneko, T. Ban, and Y. Takahashi, "Solid Solubility of SnO_2 in In_2O_3," *J. Ceram. Soc. Jpn.*, **108**, 803–6 (2000).
[11]N. Nadaud, N. Lequeux, M. Nanot, J. Jové, and T. Roisnel, "Structural Studies of Tin-Doped Indium Oxide (ITO) and $In_4Sn_3O_{12}$," *J. Solid State Chem.*, **135**, 140–8 (1998).
[12]G. B. Gonzalez, J. S. Okasinski, T. O. Mason, T. Buslaps, and V. Honkimäki, "*In Situ* Studies on the Kinetics of Formation and Crystal Structure of $In_4Sn_3O_{12}$ Using High-Energy X-Ray Diffaction," *J. Appl. Phys.*, **104**, 043520 (2008).
[13]H. M. Rietveld, "Line Profiles of Neutron Powder-Diffraction Peaks for Structure Refinement," *Acta Cryst.*, **22**, 151–2 (1967).
[14]J. Rodríguez-Carvajal, *An Introduction to the Program FullProf*, Laboratoire Léon Brillouin, CEA-CNRS, Saclay, France,version 2010.
[15]V. Honkimäki, K. Hämäläinen, and S. Manninen, "Quantitative X-Ray Fluorescence Analysis Using Fundamental Parameters: Application to Gold Jewelry," *X-Ray Spectrom.*, **25**, 215–20 (1996).
[16]G. B. González, T. O. Mason, J. P. Quintana, O. Warschkow, D. E. Ellis, J.-H. Hwang, J. P. Hodges, and J. D. Jorgensen, "Defect Structure Studies of Bulk and Nano-Indium-Tin Oxide," *J. Appl. Phys.*, **96**, 3912–20 (2004). □